Impact of Process Variability on Write Error Rate and Read Disturbance in STT-MRAM Devices

Jeehwan Song[1], Hemant Dixit[2], Behtash Behin-Aein[3], Chris H. Kim[1], and William Taylor[2]

[1]University of Minnesota, Minneapolis, MN 55455, USA
[2]GLOBALFOUNDRIES, Malta, NY 12020, USA
[3]GLOBALFOUNDRIES, Santa Clara, CA, 95054, USA

Spin-Transfer Torque Magnetic Random Access Memory (STT-MRAM) is the most promising next generation memory technology that combines the advantages of mainstream memory technologies such as SRAM, DRAM, and Flash. In the STT-MRAM, a magnetic tunnel junction (MTJ) is used as a bit-cell to store the data and its magnetic properties have critical role in thermal noise aware STT-switching operations. This work analyzes the impact of MTJ material and geometric parameter variations such as saturation magnetization (M_S), magnetic anisotropy (H_K), damping factor (α), spin polarization efficiency factor (η), oxide thickness (t_{OX}), free layer thickness (t_F), tunnel magnetoresistance (TMR), and cross-sectional area of free layer (A_F) variations on Write Error Rate (WER) and Read Disturbance Rate (RDR) for reliable write and read operations, respectively. To evaluate the scalability of MRAM devices, we investigate both WER and RDR with a wide range of MTJ diameters between 90 nm and 30 nm that corresponds to mainstream technology nodes from 40 nm up to 14 nm advance node. In our work, the Fokker-Planck (FP) numerical approach is mainly utilized for an efficient analysis, which allows for parametric variation and evaluates its impact on switching. Although the impact of material and geometric parameter variations on WER is decreased as MTJ scales down from 90nm to 30nm, the variation effect can be still critical with small MTJ diameter and the most significant influential variation is η, M_S, H_K, and α in that order. By contrast, the impact of material and geometric parameter variation on RDR increases in MTJ scaling, and we show that negative variations of H_K and M_S could be a critical bottleneck in 30nm and 40nm MTJ diameters. Our work finally emphasizes the necessity of the WER and RDR analysis by considering the parameter variation in MTJ scaling for practical STT-MRAM development.

***Index Terms*—Spin-transfer torque MRAM (STT-MRAM), Magnetic Tunnel Junction (MTJ), Fokker-Planck (FP), switching probability, Write Error Rate (WER), Read Disturbance**

I. Introduction

SPIN transfer torque magnetic random access memory (STT-MRAM) has come into the spotlight for a next generation memory application that provides a lot of advantages such as a high density of DRAM, a high speed of SRAM, a nonvolatility of Flash memory, a low energy consumption, an unlimited endurance, and a good compatibility with existing CMOS technology [1][2]. In the STT-MRAM applications, a magnetic tunnel junction (MTJ) device is used as a bit-cell as shown in Fig.1 (a). The MTJ device is composed of two ferromagnetic (FM) layers, i.e. a free and a fixed layers, and an oxide barrier between them. Applying appropriate amount of spin polarized current, which is larger than critical switching current (I_C), with an adequate pulsewidth (PW) through the MTJ device can flip the magnetization of free layer (Fig.1 (b)), and the final state of the magnetization is determined according to the current direction. For example, the magnetization of a free layer can be flipped to a parallel direction to that of a fixed layer when current flows from a bit line (BL) to a source line (SL), and the state is called as a P-state. On the other hand, it can be flipped to anti-parallel direction when the current flows from SL to BL, and the state is referred to as an AP-state. The P-state provides a low resistance (R_P) while the AP-state provides a high resistance (R_{AP}) for the MTJ device.

As standalone and embedded STT-MRAM applications have been actively researched for commercialization [2-4], the reliabilities on both write and read operations become more important in the manufacturing process. In other words, the applications should guarantee stable switching during write operation whereas they should prevent invalid switching during read operation. Therefore, it is essential to estimate the non-switching probability during write operation, as known as a write error rate (WER), and the switching probability during read operation, as known as a read disturbance rate (RDR). Basically, as the MTJ device technology scales down to a few tens of nanometer regime, MTJ switching is more sensitive due to lowered energy barrier between two states such as P- and AP-states [see (2) and Fig. 1(c)], resulting in poor reliability. In addition, both WER and RDR are significantly affected by the MTJ material and geometric parameters [5][6], and there are almost always some degree of parameter variations in the actual fabrication process. In this paper, we analyze the impact of several critical material and geometric parameter variations such as damping factor (α), spin polarization efficiency factor (η), magnetic anisotropy field (H_K), and saturation magnetization (M_S), oxide thickness (t_{OX}), free layer thickness (t_F), tunnel magnetoresistance (TMR), and cross-sectional area of free layer (A_F) variations on WER and RDR in MTJ scaling. Although write and read operations are influenced by MTJ scaling and the parameter variations of the MTJ device at the same time, there is still a lack of research simultaneously dealing with the effects on the operations. Since our study shows the correlation between scaling and the parameter

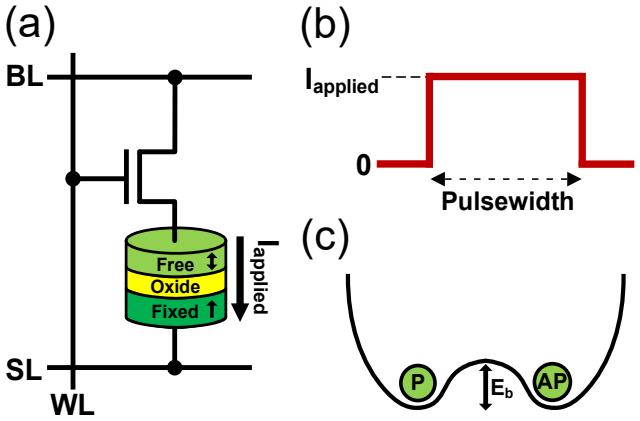

Fig. 1 (a) MTJ device structure as a bit-cell of STT-MRAM. (b) Current pulse applied for STT-switching (c) Energy barrier and magnetization states (P- and AP-states) of the MTJ free layer.

variations for WER as well as RDR, it can provides comprehensive insights for designing the practical STT-MRAM applications. To analyze in a highly efficient way, we mainly use Fokker-Planck (FP) approach that will be introduced in the following section.

The rest of the paper is organized as follows. Section II introduces the physics of the MTJ device and its magnetization dynamics during switching operation. Section III describes FP solutions including analytical and numerical solutions. We investigate the impacts of MTJ scaling with material and geometric parameter variations for both the WER in Section IV and the RDR in Section V, followed by the conclusions in Section VI.

II. MTJ Physics for STT-Switching

A. Perpendicular Magnetic Tunnel Junction

The MTJ device can be classified by the magnetic anisotropy which indicates the preferred direction of magnetization, also known as easy-axis. For example, an in-plane MTJ (I-MTJ) has an easy axis aligned to the plane of the magnetic free layer, while a perpendicular MTJ (P-MTJ) has an easy-axis perpendicular to the plane of magnetic free layer. In the absence of the demagnetization field (H_d), P-MTJ provides faster switching at lower power than I-MTJ. Furthermore, P-MTJ shows better scalability in terms of both the diameter and thickness scaling [7][8]. Due to the advantages, P-MTJ is a preferred choice of MRAM manufacturers and hence we also focus on P-MTJ device with cylindrical symmetry in the work. It should be noted that our approach can be easily extended to study of I-MTJs.

B. Thermal Stability Factor

As a nonvolatile memory application, MTJ devices must maintain the stored data for an extended time period that widely varies depending on the target application [9][10]. For example, MRAM as a main memory to replace Flash memory requires around 10 years of data retention, while the MRAM-based cache memory needs to store data for about 30 days – owing to the periodic refresh cycles in cache memories. Thermal stability factor (TSF), also denoted by Δ, of the MTJ device is an important parameter determining the data retention capability of the free layer. The stability of the magnet shows exponential dependence on the TSF and is governed by the following equation [11]:

$$t_{retention} = t_0 e^{TSF} \quad (1)$$

where $t_{retention}$ is the data retention time, and t_0 is the time for a thermally activated reversal also known as the inverse attempt frequency. Within Macrospin approximation t_0 is calculated as: $t_0 = 1 + \alpha^2/\alpha\gamma H_k$, where α is damping coefficient, H_k is anisotropy field and γ is the gyromagnetic ratio.

A higher energy barrier of the MTJ device more stabilize the magnetization in current status, resulting in longer retention time. Since the TSF is a ratio of free layer's energy barrier to thermal energy (k_BT) as expressed in (2), it is proportional to the data retention time of the MTJ device [12].

$$TSF = \frac{E_b}{k_BT} = \frac{\mu_0 H_K M_S V_F}{2k_BT} \quad (2)$$

where the E_b is the energy barrier, k_B is the Boltzmann constant, T is the absolute temperature, μ_0 is the permeability in vacuum, H_K is the anisotropy field, and temperature dependence $M_s = M_{s0}(1 - T/T_c)^{\beta}$ where M_{s0} is the saturation magnetization at the temperature of 0K, T_c is the Curie temperature, β is material-dependent constant

C. Magnetization Dynamics

The MTJ free layer's magnetization dynamics can be described by solving stochastic Landau-Lifshitz-Gilbert (sLLG) equation which consists of precession, damping, and spin transfer torque terms as expressed as follows [13].

$$\frac{1+\alpha^2}{\gamma} \cdot \frac{d\vec{M}}{dt} = -\vec{M} \times \vec{H}_{eff} - \alpha \cdot \vec{M} \times \left(\vec{M} \times \vec{H}_{eff}\right) + \frac{\hbar P J}{2e t_F M_s} \cdot \vec{M} \times \left(\vec{M} \times \vec{M}_P\right) \quad (3)$$

where α is the Gilbert damping constant, γ is the gyromagnetic ratio, $\vec{M}$ is the magnetization vector of the free layer, $\vec{H}_{eff}$ is the effective magnetic field, $\hbar$ is the reduced Planck's constant, P is the spin polarization, J is the switching current density, e is the electron charge, t_F is the free layer thickness, and $\vec{M}_P$ is the magnetization vector of fixed layer. In detail, $\vec{H}_{eff}$ consists of different fields as follows.

$$\vec{H}_{eff}(V) = \vec{H}_K + \vec{H}_d + \vec{H}_{ext} + \vec{H}_{th} \quad (4)$$

Here, $\vec{H}_K$ is the magnetic anisotropy field, $\vec{H}_d$ is the demagnetization field, $\vec{H}_{ext}$ is the external magnetic field, and $\vec{H}_{th}$ is the thermal field. To add thermal noise-induced stochasticity to the magnetization's transient behavior, the thermal field is assumed as a zero-mean Gaussian distribution with standard deviation ($\sigma_{H_{th}}$) characterized as below [14].

$$\sigma_{H_{th}} \propto \sqrt{\frac{2k_B\alpha T}{\mu_0\gamma V_F M_s}} \quad (5)$$

In addition, the thermal noise also affects to an initial angle

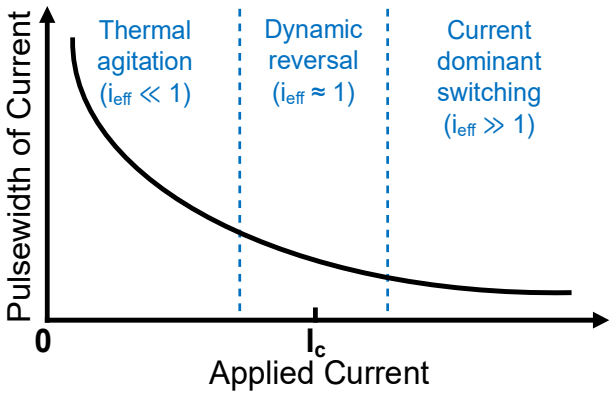

Fig. 2. Switching current regimes: thermal agitation, dynamic reversal, and current dominant switching regimes

of the magnetization, thus the initial angle's probability distribution can be modeled as follows [15].

$$PDF(\theta)|_{t=0} = \frac{exp(-TSF\cdot\sin^2\theta)}{\int_0^{\pi}\sin\theta\, exp(-TSF\cdot\sin^2\theta)\, d\theta} \quad (6)$$

Here, $PDF(\theta)|_{t=0}$ is the initial angle's probability distribution function, and θ is the magnetization's angle.

Even though the sLLG solution can mimic more accurate physics-based magnetization dynamics, by keeping track of magnetic trajectory, it is obvious that the solution requires substancsctially long simulation time and large computational resources. For example, if one needs to determine WER or RDR using sLLG equation, a large number of trials with different contributions from the thermal noise are necessary to capture the stochastic nature of the magnetization's physical behavior. Typically, commercial memory applications need WER or RDR to be lower than or equal to 10^{-9} [16-19]. Thus, at least 10^9 sLLG simulation runs with a distribution of the initial magnetization angle and thermal noise are required. Although it is possible in principle, it leads to huge computational time ranging over days to months.

Alternatively, computationally efficient approach to determine the WER or RDR is provided by the FP equations equation. Within the FP approach, instead of keeping track of magnetic trajectories during switching, one is concerned with probability of non-switching. Since the FP equation describes an equation of motion for the probability density, it is computationally much more efficient and can be easily solved using standard programing languages such as MATLAB, Python, and C codes. The manifestation of the FP equation to describe the magnetization density is discussed in the following section.

III. Fokker-Planck Solutions

The generalized FP equation in statistical mechanics describes the time evolution of the probability density function of the velocity of the particle under influence of the drift and diffusion terms. The one dimensional time independent FP in general terms is given by:

$$\frac{\partial\rho(x,t)}{\partial t} = -\frac{\partial}{\partial x}D^{(1)}(x)\rho + \frac{1}{2}\frac{\partial^2\rho(x,t)}{\partial^2 x}D^{(2)}(x)\rho \quad (7)$$

TABLE I
Material and Geometric Parameters for Simulation Work

Parameter	Description	Default Value
CD	Critical diameter of MTJ	30-90 nm
t_F	Thickness of free layer	1.0 nm
t_{OX}	Thickness of oxide barrier	0.85 nm
α	Damping factor	0.033
M_{S0}	Saturation magnetization at 0K	8.65×10^5 A/m
η	Spin polarization efficiency factor	0.6
H_K	Magnetic anisotropy	3.024×10^5 A/m
RA	Resistance-area product	18 Ω·μm^2
TMR	Tunnel magnetoresistance	160 %
T	Temperature	300 K

where ρ is the probability density, $D^{(1)}(x)$ is the drift or convection term, and $D^{(2)}(x)$ is the diffusion term. When we talk of the magnetization reversal of the free layer of the MTJ, the probability distribution of the magnetic moment is conserved. Thus, the FP equation can also be used to describe the time evolution of the magnetic moment under STT switching (representing drift) and the thermal noise (leading to diffusion) [15]. Further, the WER estimate is a finding the probability of magnetic moment pointing in parallel or anti-parallel orientation and hence the integral of FP equation yields the probability of switching as a WER.

The FP equation for the thermal noise aware STT-switching requires only a single simulation run to obtain the necessary WER, thus it takes extremely short simulation time compared to sLLG solution explained in Section II-C [6]. Despite there is a tradeoff between an accuracy of the sLLG solution and an efficiency of the FP solution, both solution results show coterminous results [5][20]. Especially, for the case of P-MTJ with cylindrical symmetry, the FP equation can be simplified to 1D differential equation form, as a result it can be readily solved in analytical or numerical way [5]. In the rest of the Section, both analytical and numerical solutions for STT-switching of P-MTJ will be described.

A. Fokker-Planck Analytical Solution

As shown in Fig. 2, the switching current can be classified into three different regimes according to the effective current ratio ($i_{eff} = I_{applied}/I_c$) where the $I_{applied}$ is the applied current through the MTJ device [21][22]: current dominant switching regime when the $I_{applied}$ is much higher than I_c ($i_{eff} \gg 1$), thermal agitation regime when $I_{applied}$ is much lower than I_c ($i_{eff} \ll 1$), and dynamic reversal regime that are affected by thermal noise and spin current at the same time when $I_{applied}$ is near to I_c ($i_{eff} \approx 1$). Within the Macrospin approximation which means the magnetic moment of free layer does not change in time and thereby exhibit a coherent switching of the entire volume, the I_c can be described using MTJ material and geometric parameters as follows.

$$I_c = \frac{2\alpha e}{\eta\hbar}\mu_0 H_K M_s V_F \quad (8)$$

According to the regimes, different FP analytical solutions should be applied. For example, in the current dominant

This article has been accepted for publication in a future issue of this journal, but has not been fully edited. Content may change prior to final publication. Citation information: DOI 10.1109/TMAG.2020.3028045, IEEE Transactions on Magnetics

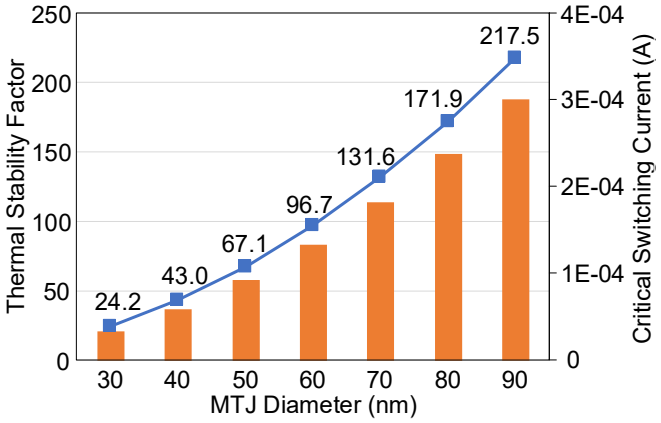

Fig. 3. Thermal stability factor and critical switching current, within the Macrospin approximation, for different MTJ diameters.

switching regime, the FP analytical solution for WER estimate with a given PW can be expressed as follows [23].

$$WER(t) = 1 - exp\left[\frac{-\pi^2 \cdot TSF \cdot (i_{eff}-1)/4}{i_{eff} \cdot \exp(2\alpha\gamma \cdot H_K \cdot t(i_{eff}-1)/(1+\alpha^2)) - 1}\right] \quad (9)$$

where t is the time delay that represents a PW of the applied current. Meanwhile, in the thermal agitation regime, the FP analytical solution can be modeled as below [15].

$$WER(t) = 1 - t\sqrt{\frac{TSF}{\pi}}\left(1 - i_{eff} + h\right)^2 \cdot \left(1 + i_{eff} - h\right) \cdot \exp[-TSF\left(1 - i_{eff} + h\right)^2] \quad (10)$$

where h is the normalized external magnetic field calculated as $h = H_{ext}/H_K$.

However, there are additional considerations when utilizing the FP analytical solutions. The solutions should be carefully utilized with consideration for the different regimes, since (9) and (10) are only valid for current dominant regime and thermal agitation regime respectively. Moreover, there is no specific analytical solution for the dynamic reversal regime although the regime is useful for low power MTJ switching. Therefore, the FP analytical solution is not only ineffective but also insufficient when considering entire switching regimes.

B. Fokker-Planck Numerical Solution

More efficiently, the simplified 1D differential equation form of FP equation for magnetization dynamics can be numerically solved using a partial differential equation as follows [5][15].

$$\frac{\partial \rho}{\partial t} = -\nabla(L\rho) + D\nabla^2\rho \quad \text{where } D = \frac{\alpha\gamma k_B T}{(1+\alpha^2\mu_0 M_S V)} \quad (11)$$

Here L is the sum of all the effective STT torques and D is the effective diffusion coefficient representative of the thermal noise.

For efficient STT switching, the non-collinearity of the magnetic moments of free and reference layer is also necessary and hence the evolution of the magnetization density critically depends upon the initial angle between these moments. Thus, the 1D FP equation can also be written in terms of initial angle as follows:

$$\frac{\partial \rho(\theta,\tau)}{\partial \tau} = -\frac{1}{sin\theta}\frac{\partial}{\partial \theta}\left(sin^2\theta(i_{eff} - h - cos\theta)\rho(\theta,\tau) - \frac{sin\theta}{2 \cdot TSF}\frac{\partial \rho(\theta,\tau)}{\partial \theta}\right) \quad \text{where } \tau = \frac{\alpha\gamma\mu_0 H_K}{1+\alpha^2}t \quad (12)$$

Here, θ is the angle of the magnetization from an easy axis (+z-axis), τ is the normalized time, and $\rho(\theta,\tau)$ is the probability that the magnetization is pointing to the angle θ at τ.

Basically, (12) is a continuity equation indicating the probability density change of θ over time, and it can generalize the thermally noisy magnetization switching with STT effect. Since the FP numerical solution can cover entire switching regimes without any discontinuity, it can overcome the limitations of the FP analytical solution. In addition, the FP numerical solution is proven that it sufficiently well reproduces the experimental measurement for all the switching regimes [5]. Due to the advantages, we will mainly use the FP numerical solution to explore WER and RDR.

The angle of $\pi/2$ is used as a criterion to determine the completion of the magnetization switching. For instance, in case of the initial P-state, the non-switched magnetization indicates θ remains in the range between 0 and $\pi/2$ after applying current pulse, while the switched magnetization indicates θ goes over to the range between $\pi/2$ and π. Therefore, the ratio of non-switched magnetization can be used for WER as below.

$$WER = \int_0^{\pi/2} \rho(\theta;\tau)d\theta \quad (13)$$

On the contrary, the RDR can be described by the ratio of switched magnetization as follows.

$$RDR = \int_{\pi/2}^{\pi} \rho(\theta;\tau)d\theta = 1 - \int_0^{\pi/2} \rho(\theta;\tau)d\theta \quad (14)$$

Using the equations explained in Section II and III, we can efficiently analyze the impact of MTJ material and geometric parameter variations on WER and RDR estimates in the rest of the paper. Note that both WER and RDR actually depend not only MTJ device itself but also on the write and read peripheral circuitry. Moreover, the PVT variations of the transistors used in the read and write circuitry can also have an influence on the error rates. To improve the error rates, various types of variation-aware write and read circuits have actively proposed from both academia and industry [24-27]. Nevertheless, understanding MTJ's intrinsic characteristics such as the effects of material and geometric parameter variations on the error rates in is still invaluable and it can provide a guidelines for designing the specific read/write circuits based on the MTJ's characteristics analyzed by FP numerical model.

IV. Investigation of Write Error Rate

As a MTJ device technology has been scaled down from 90nm to 30nm regime, both TSF and I_C, which play important roles in the MTJ physical behavior, are considerably decreased (Fig. 3). Due to the decrease of the parameters, smaller MTJ can

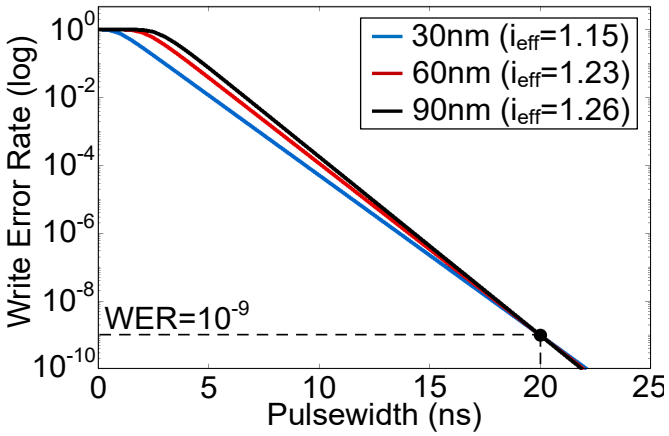

Fig. 4. Write error rate as a function of PW for different MTJ diameters (30nm, 60nm, 90nm). Effective current ratio is optimized to obtain WER of 10^{-9} with 20ns PW for each diameter.

provide faster switching and lower switching energy consumption. On the other hand, smaller MTJ can be more sensitive to the thermal noise, resulting in degradation of WER. Therefore, an accurate estimate of WER has become more important in MTJ scaling to guarantee reliable write operations. In reality, the fabrication process of MTJ device has necessarily generated a certain amount of material and geometric parameter variations and the standard deviation is about ±10%, as observed empirically through the process capability index (Cp). From (2) and (8), the variations of the key material and geometric parameters such as α, η, H_K, M_S, t_F, A_F, and TMR have substantial effect on TSF and I_C. As a result, we should consider the material and geometric parameter variations as well as MTJ scaling in WER estimate.

Previously, various researches about the WER and RDR were implemented. For example, the sensing margin and read disturbance was studied considering process variation [25], and the tradeoff between RDR and read current was investigated [41]. In addition, the effect of process variations on WER was analyzed using FP numerical [5][6] and analytical models [23]. Compared to the previous ones, our FP-based research deals with both WER and RDR considering diverse process variations as well as MTJ downscaling at the same time.

For a more realistic physics-based MTJ device model, the most parameters in our work are chosen based on the experimental data of CoFeB/MgO/CoFeB P-MTJ [28]. Table I shows the experiment-based parameter values, and different MTJ diameters from 30nm to 90nm at intervals of 10nm are used in order to analyze the effect of MTJ scaling. A target PW for the applied current is set up to 20ns [29][30]. Depending on the MTJ diameter, i_{eff} should be optimized to obtain the WER of 10^{-9} with the target PW. As shown in Fig.4, for example, i_{eff} should be 1.15 for 30nm diameter, 1.23 for 60nm diameter, and 1.26 for 90nm diameter. Based on the initial setup, the material and geometric parameter variations of ±10% are applied for simplicity, and the change of required PW to obtain WER of 10^{-9} is analyzed.

A. The Impact of MTJ material parameter variation

The impact of key material parameter variations such as α, η, H_K, and M_S variations on WER is analyzed by using (8) and (13). To obtain the impact on WER, the value of $I_{applied}$ is maintained regardless of the material parameter variations. As mentioned in previous Section, the magnetization switching is affected by both I_C and TSF, but the impact of material parameter variation on WER can be mainly understandable by the equation of I_C. This is because the write current pulse is positioned in the dynamic reversal regime where I_C is considered as a more critical factor than TSF (Fig.2).

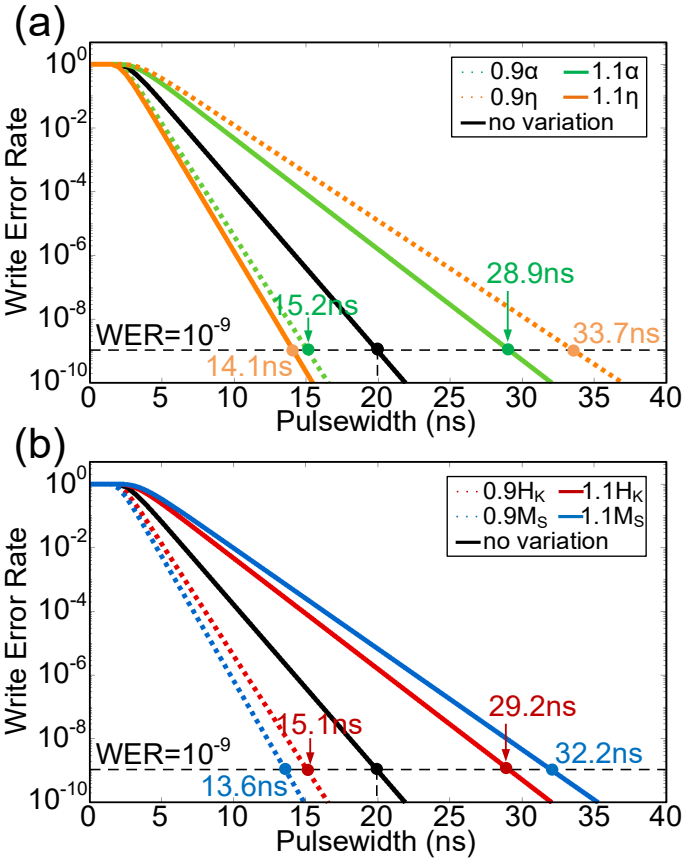

Fig. 5. Sense error rate as a function of PW including 90nm MTJ material parameter variations. (a) Damping factor and spin polarization efficiency factor variations. (b) Magnetic anisotropy field and saturation magnetization variations

Firstly, we analyze the effect of damping factor, α, variation on WER. Basically, α describes the relaxation rate of the magnetization to equilibrium [31]. Although the α is composition-dependent material constant for thin films, it increases at lower thickness (typically below 2nm). In Fig. 5 (a), the impact of α variation on WER for 90nm diameter is indicated. The required PW to obtain WER of 10^{-9} is 28.9ns when α increases by 10%, while the PW is 15.2ns when α decreases by 10%. Since α forces the magnetization toward the opposite direction to the STT effect until the moment when θ reaches $\pi/2$, the magnetization switching is more disturbed by a larger α.

Secondly, the effect of spin polarization efficiency factor, η, variation is studied. The parameter η represents the degree of the magnetization's switching efficiency. In other words, higher η enables magnetization to switch more easily. The impact of η variation on WER for 90nm diameter is shown in Fig. 5 (a). The required PW is 14.1ns when η increases by 10%, while the PW

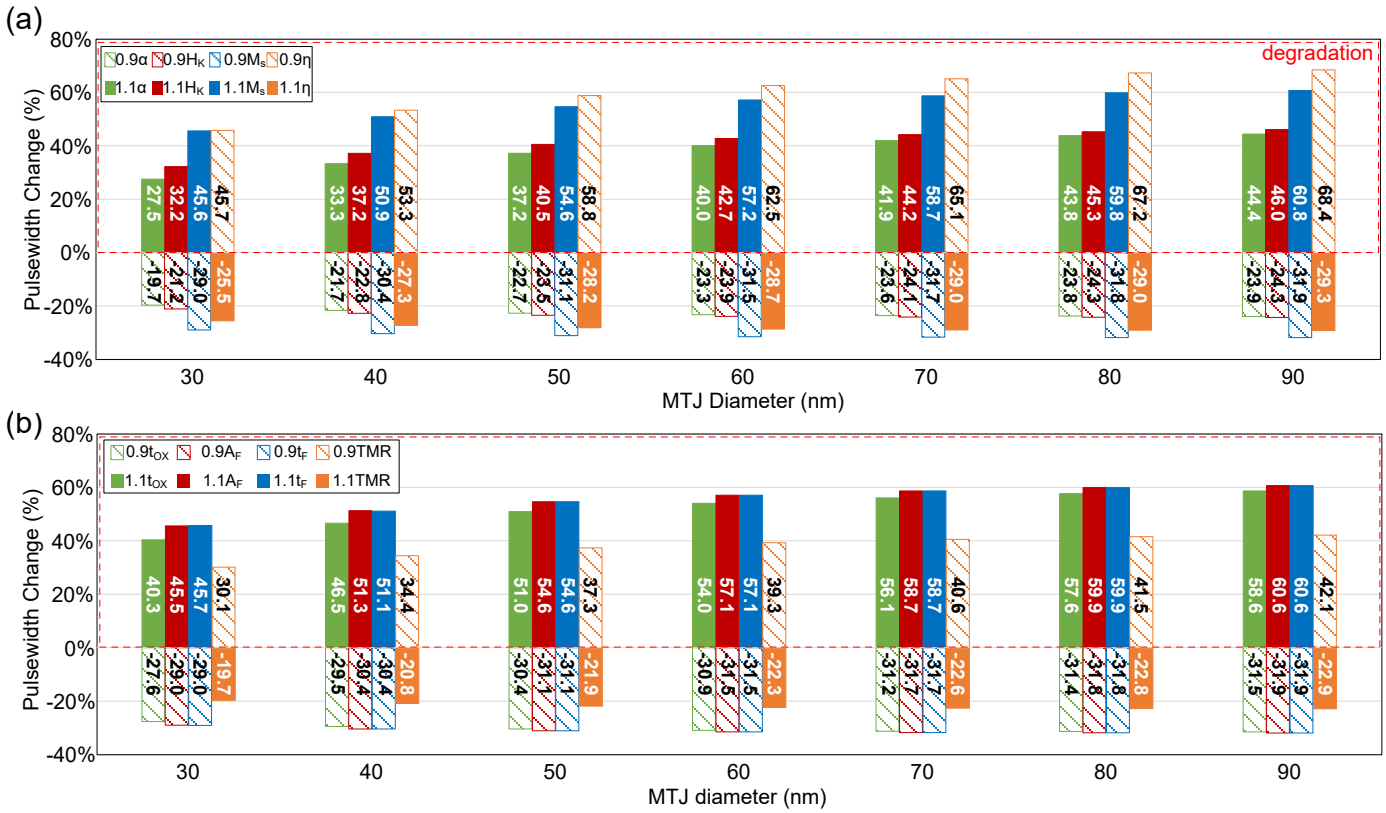

Fig. 6 (a) Percentage change of the PW to meet WER of 10^{-9} with material parameter variations for different MTJ diameters. (b) Percentage change of the PW to meet WER of 10^{-9} with geometric parameter variations for different MTJ diameters.

is 33.7ns when η decreases by 10%.

Thirdly, we analyze the magnetic anisotropy field, H_K, introduced in Section II-A. Since H_K compels magnetization to stay its initial state, larger current or longer PW is required to tilt the magnetization when higher H_K is applied. Fig. 5 (b) includes the impact of the H_K variation on WER for 90nm diameters. The required PW is 29.2ns when H_K changes by +10%, while the PW is 15.1ns when H_K changes by -10%.

Lastly, the effect of saturation magnetization, M_S, variation is investigated. As shown in Fig. 5 (b), the required PW is 32.2ns with +10% of M_S variation whereas the PW is 13.6ns with -10% of the variation. The parameter M_S represents the maximum possible value completing the alignment of magnetic moment vector towards the direction of magnetic field, thus larger current or longer PW is needed to complete the magnetization flipping when applying larger M_S.

B. The effect of MTJ device scaling

A STT-switching is affected by MTJ scaling as well as the material parameter variation. Fig. 6 (a) shows the impact of all material parameter variations for different MTJ diameters from 30nm to 90nm at intervals of 10nm. The PW change (ΔPW) in percentage terms, which indicates a ratio of the changed PW for WER of 10^{-9} to the target PW of 20ns, is used as a scale.

Overall, the impact of all material parameter variations on WER decreases as the MTJ diameter scales down from 90nm to 30nm. This is because both I_C and TSF are proportional to the volume of MTJ device as expressed in (2) and (8). Even though the MTJ scaling diminishes the impact of material parameter variations, the impact on WER is still considerable even in the 30nm diameter. As a positive ΔPW means a degradation of WER, especially the positive ΔPW should be more carefully investigated for a reliable write operation. Based on the results, regarding the positive ΔPW, the most significant influential material variation is η, M_S, H_K, and α in that order. Consequently, the design considering relative importance of the material parameter variations is necessary to guarantee the stable write operation in STT-MRAM application. Note that the ΔPW always have some degree of differences according to the material parameters at each MTJ diameter. This is due to the fact that not only I_C but also the correlation with TSF and τ can affect to the switching operation as indicated in (12).

C. Effect of Geometrical Parameter Variation in WER

During a manufacturing process of the P-MTJ, there is a high possibility of existing variations on the geometric parameters such t_{OX}, t_F, TMR, and A_F [32-36]. We analyze the effect of the geometric parameter variations on WER using the FP numerical model.

First, the oxide barrier thickness, t_{OX}, changes the resistance of MTJ as expressed in the equation follows [34][37].

$$R_P = \frac{t_{OX}}{F \times A_F \times \sqrt{\varphi}} \times \exp\left(1.025 \times t_{OX} \times \sqrt{\varphi}\right) \qquad (15)$$

where F is the fitting factor calculated from the RA of the MTJ, φ is the oxide energy barrier height. Thicker t_{ox} allows lesser tunnel current through it due to increased R_P, which means that

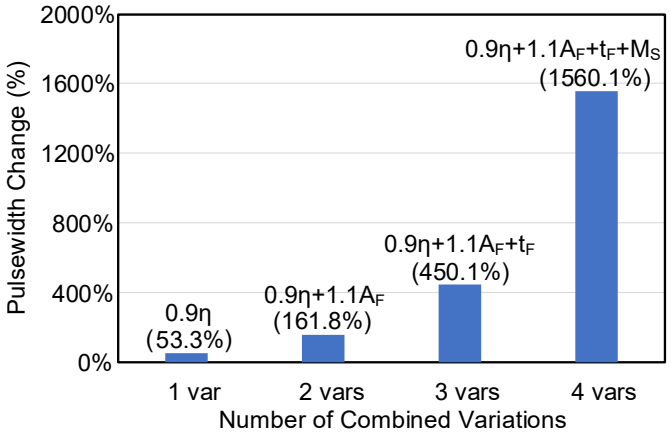

Fig. 7. Pulsewidth change with the combination of parameter variations at 40nm MTJ diameter.

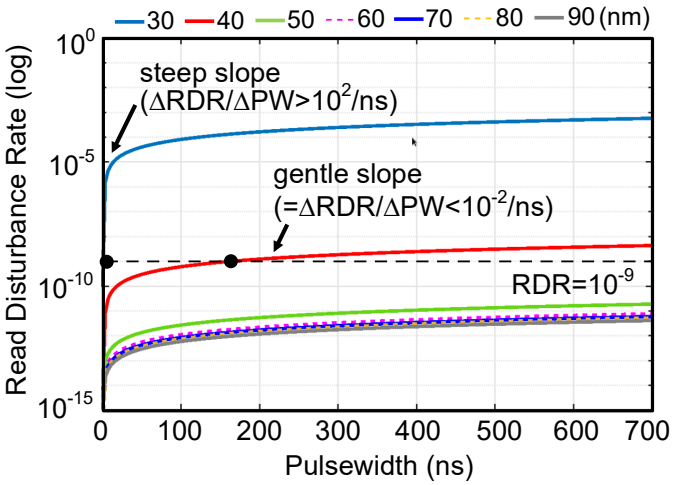

Fig. 8. Read disturbance rate as a function of PW for different MTJ diameters.

longer PW or higher current is needed to switch the MTJ. Second, the cross-sectional area, A_F, affects the switching operation. From (15), it can be inferred that increasing A_F induces larger current through MTJ owing to reduced R_P. However, both I_C and TSF, which have critical roles in MTJ switching, are increased according to the expansion of A_F due to increase of V_F in (2) and (8). Consequently, expanded A_F in MTJ requires longer PW or higher current for switching operation. Third, the impact of the free layer thickness, t_F, is also investigated. Since V_F is also proportional to t_F, the impact of t_F is very similar to the effect of A_F. In other word, MTJ with thicker t_F requires nearly the same degree of longer PW or higher current to flip MTJ. Lastly, the impact of TMR on switching operation is studied. The TMR can change the spin polarization efficiency factor, η, by correlation between TMR, P, and η as follows [38][39].

$$\eta(\theta) = \frac{P}{2(1+P^2\cos\theta)}, \quad P = \sqrt{\frac{TMR}{2+TMR}} \tag{16}$$

Here, θ is the angle between the magnetizations of free and fixed layers. Since higher η can be obtained with larger TMR, MTJ with larger TMR can provide faster switching operation [35][40].

As shown in Fig. 6 (b), the impact of the geometric parameter variations for different MTJ diameters is obtained by using same approach mentioned in Section IV-A. Analogous with the material parameter variations, the impact of geometric parameter variations on WER decreases as the MTJ diameter scales down. Considering the degradation of ΔPW, the most influential geometric variation is A_F (≈t_F), t_{OX}, and TMR in that order, and the relative importance of the material parameter variations should be considered in design process. Furthermore, we evaluate the worst case of WER with combined variations of material and geometric parameters. In Fig. 7, all combinations are chosen to evaluate the worst case of WER degradation at each variation number. The ΔPW exponentially increases with combining degraded variations, due to multiplication of the effects of degradation sources. We include maximally four variations for the worst case analysis since it was enough to show the effects of the multiple variation sources. Even if MTJ scaling can diminish the impact of each material or geometric variation, the combined degradation might be relatively critical to the error rates. Consequently, precise manufacturing process to reduce variations and variation-aware circuit design are both essential for stable write operation.

V. Analysis of Sensing Error Rate

A. Read Disturbance and Sensing Margin

Two different types of errors exist in read operation of STT-MRAM application: read disturbance and low sensing margin. The read disturbance is an unwanted MTJ flipping during read operation, and only 20% of I_C is generally used as a read current to prevent the read disturbance [41]. In spite of the low read

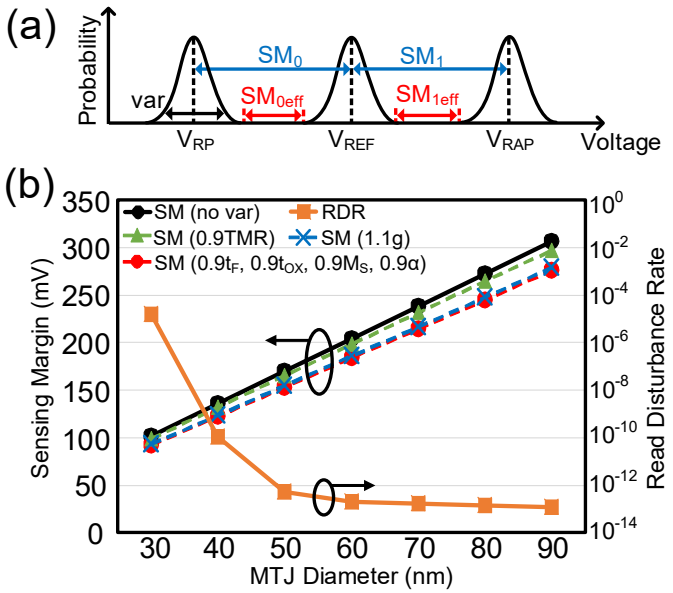

Fig. 9. (a) Concept of target sensing margin (SM_0 and SM_1) and effective sensing margin (SM_{eff0} and SM_{eff1}) due to variations, (b) Sensing margin trend and read disturbance as technology scaling. Sensing margin degradation caused by MTJ processing variations are included, and the sensing time is set up to 20ns for obtain RDR [30].

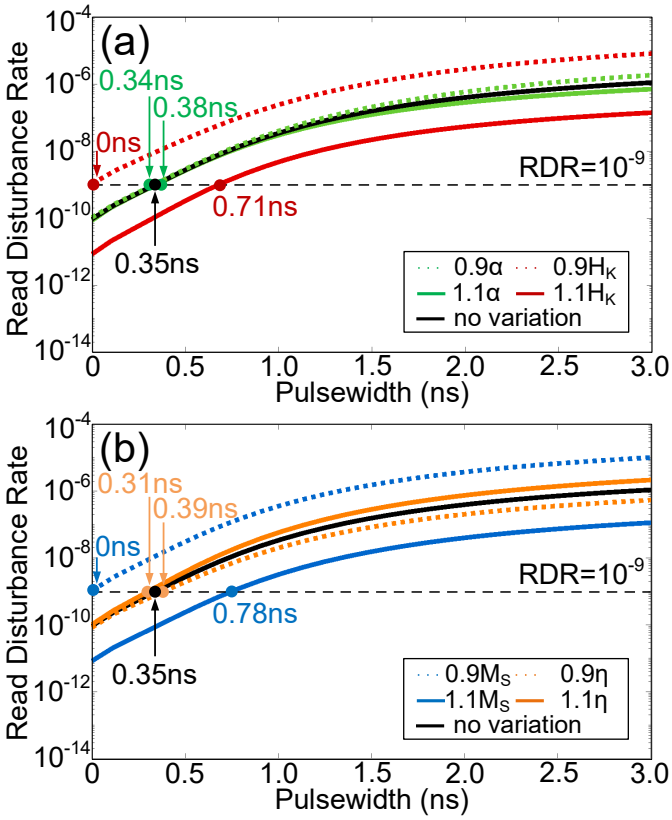

Fig. 10. Read disturbance rate as a function of PW including 30nm MTJ material parameter variations. (a) Damping factor and magnetic anisotropy field variation. (b) Saturation magnetization and spin polarization efficiency factor variations.

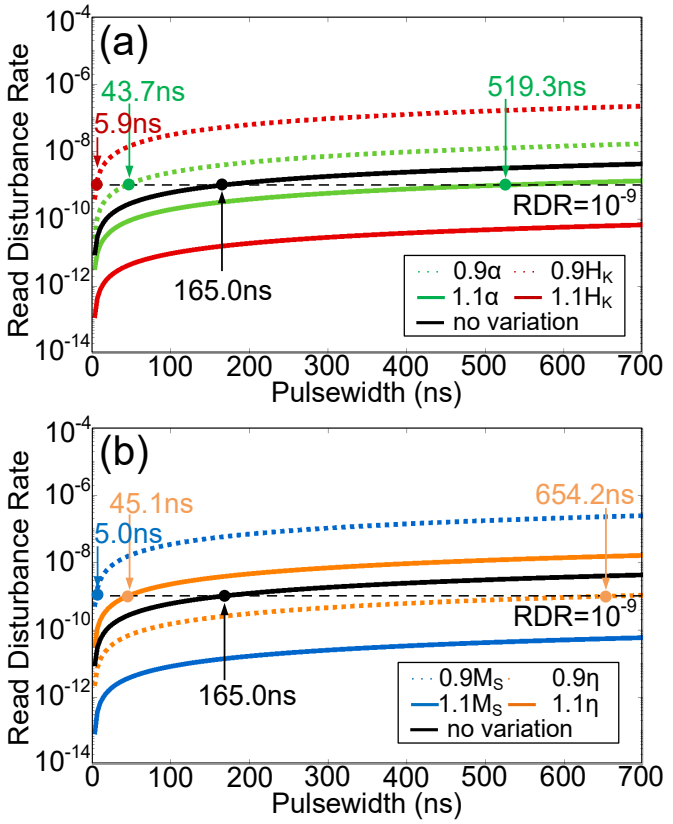

Fig. 11. Read disturbance rate as a function of PW including 40nm MTJ material parameter variations. (a) Damping factor and magnetic anisotropy field variation. (b) Saturation magnetization and spin polarization efficiency factor variations.

current, as shown in Fig. 8, the smaller MTJ device provides larger RDR since there are chances to accidently flip the magnetization due to lowered TSF in MTJ scaling. Since the MTJ device whose diameter is equal to or larger than 50nm provides the RDR sufficiently lower than 10^{-9} with long PW (i.e. 300ns), we focus on an investigation of the RDR with 30nm and 40nm MTJ diameters. In addition, the required PW to meet RDR of 10^{-9} for 30nm diameter is located in the steep slope region, whereas the PW for 40nm diameter is located in the gentle slope region (Fig. 8). For simplicity, we define the steep slope (=ΔRDR/ΔPW) is larger than 10^{2}/ns while the gentle slope is lower than 10^{-2}/ns. As discussed later in the Section, the impacts of MTJ material and geometric parameter variations are substantially different depending to the slope region.

A low sensing margin is another concern to make an error in read operation. In typical current or voltage sensing circuits of STT-MRAM applications, the state of the selected MTJ cell is sensed by current or voltage difference between selected MTJ and reference MTJ cells, as known as sensing margin, and it is described in Fig. 9(a). The sensing margin is expressed as follows[42][43].

$$SM_0 = V_{REF} - V_{R_P} \; and \; SM_1 = V_{R_{AP}} - V_{REF} \qquad (17)$$

Here, SM_0 is the voltage difference between reference voltage (V_{REF}) and the voltage of R_P state (V_{R_P}), SM_1 is the voltage difference between reference voltage (V_{REF}) and the voltage of R_{AP} state ($V_{R_{AP}}$), and the V_{REF} is defined as $(V_{R_{AP}} + V_{R_P})/2$. As described in Fig. 9(a), the effective sensing margin can be reduced due to variations.

The sensing margin is basically proportional to the product of applied current and MTJ resistance and a sufficient sensing margin is needed for reliable sensing operations. As MTJ device scaling, the resistance of the P-MTJ device increases as experimentally proven in [15], however a lower read current is applied to suppress the read disturbance, resulting in difficulty to ensure the adequate sensing margin [30]. As shown in Fig. 9 (b), we briefly analyzed the sensing margin trend in technology scaling and the effect of MTJ processing variations, considering an appropriate scaling scenario from 90nm to 30nm. As technology scales down, the sensing margin decreases and even more with the variations, on the other hand, the RDR increases as technology scaling. Therefore, the trends of sensing margin and RDR will lead an increase of the read failure rate as technology scaling [37].

Increasing resistance and TMR of the MTJ device can be simple alternatives to improve the sensing margin [41]. Although, theoretically, very high values of TMR (~1200%) are possible across standard Fe-MgO based MTJ's, the Physical Vapour Deposition (PVD) process as required by the high volume manufacturing, typically restricts best TMR values with best TMR reported are ~180-200% for RA of 8-12 Ohm/cm^2 [44]. This implies that a fundamental understanding of RDR at both intrinsic device and at circuit level is important. We want to stress the fact that, the sensing margin is determined not only by the material and geometric parameters of MTJ device but also circuit parameters of the sense amplifier. For example,

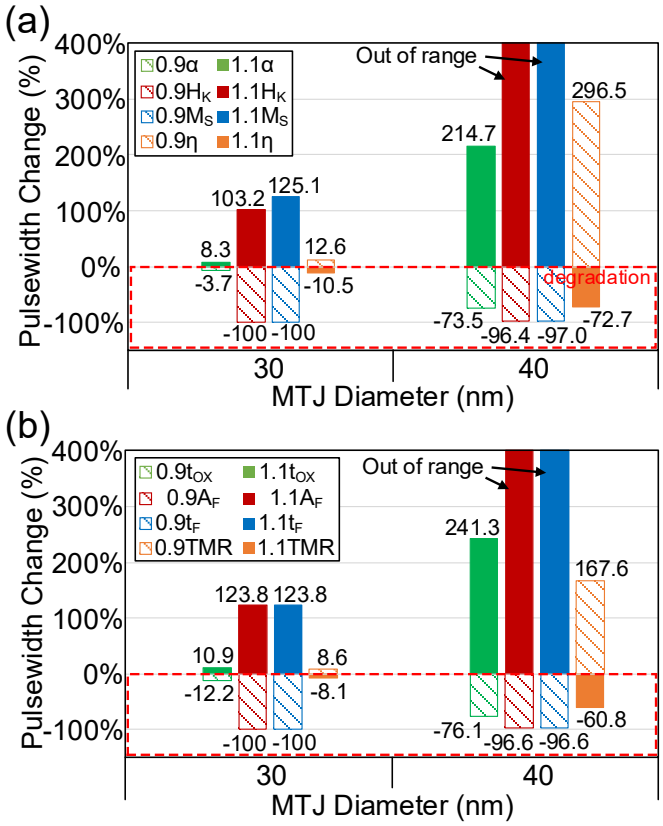

Fig. 12. (a). Percentage change of the PW to meet RDR of 10^{-9} with material parameter variations for 30nm and 40nm MTJ diameters. (b) Percentage change of the PW to meet RDR of 10^{-9} with geometry parameter variations for 30nm and 40nm MTJ diameters.

increasing PVT variations of the transistor with CMOS technology scaling can significantly reduce the sensing margin [37]. However, a circuit level analysis considering the sense amplifier is beyond the scope of this study and we focus on device level analysis using the FP numerical model and provide the valuable insights.

B. Impact of Material Parameter Variation in Different Slope Regions

The impact of MTJ material parameter variations on RDR is investigated with (14). For read operations, $I_{applied}$ is fixed by 20% of I_C at each MTJ diameter regardless of material parameter variations. Similar to WER analysis, we primarily study the required PW to meet RDR of 10^{-9} with applying the variations of ±10% for all material parameters such as M_S, H_K, α, and η. During RDR analysis, TSF is relatively more important factor than I_C since the read current pulse is located in thermal agitation regime (Fig. 2).

Firstly, we investigate the impact of material parameter variations on RDR with 30nm MTJ diameter. Initially, as shown in Fig. 10, the required PW is 0.35ns without any variation. Fig. 10 (a) indicates the impact of the H_K variation on RDR. The required PW is 0.71ns when H_K increases by 10% while it is 0ns when H_K decreases by 10%. Since TSF is proportional to H_K as expressed in (2), lower H_K enables magnetization to switch faster whereas higher H_K makes magnetization to switch slower. In Fig. 10 (a) also shows the impact of α variation on RDR. The required PW is 0.38ns with

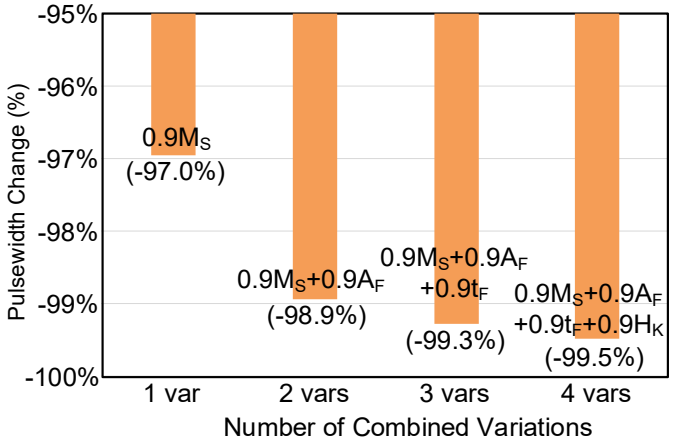

Fig. 13. Pulsewidth change with the combination of parameter variations at 40nm MTJ diameter. (All combinations are chosen to evaluate the worst case of RDR degradation at each variation number.)

+10% of α variation, while the PW is 0.34ns with -10% of the variation. Due to the relation between α and I_C in (8), lower α helps magnetization switching while larger α disturbs the switching. However, the amount of the change in RDR is relatively smaller than the change in WER, because the I_C is less critical factor in thermal agitation regime during read operation.

In addition, considering the η variation, the required PW is 0.31ns when η changes by +10%, whereas the PW is 0.39ns when η changes by -10% (Fig. 10 (b)). This is based on that I_C is inversely proportional to η as mentioned in Section IV, yet the impact of α variation is subtle due to the weak influence of I_C in read operation. Fig. 10 (b) also includes the impact of M_S variation on RDR. The required PW is 0.78ns with 10% increase in M_S, while it is 0ns with 10% decrease in M_S. This is because M_S is direct proportional to TSF as written in (2), thus lowered M_S provides lower TSF, resulting in faster switching. Based on the results, it is an undeniable fact that the -10% variations of H_K and M_S can be serious bottlenecks for stable read operation with 30nm MTJ diameter.

Next, we analyze the impact of material parameter variation on RDR in 40nm MTJ diameter. The required PW without any variations is 165.0ns. Fig. 11 (a) shows the impact of H_K and α variations on RDR. The required PW is outside of the tested range (i.e. >700ns) when H_K increases by 10%, while the PW is 5.9ns when H_K decreases by 10%. Although the H_K variation impact in 40nm MTJ diameter has a same trend with the impact in 30nm diameter, the quantity of the ΔPW in 40nm diameter is much larger than that in 30nm diameter. Regarding the α variation, the required PW is 519.3ns with +10% of α variation, whereas it is 43.7ns with -10% of α variation.

Fig. 11 (b) includes the impact of η and M_S variations. The required PW is 45.1ns with +10% of η variation, while the PW is 654.2ns with -10% of the variation. When M_S increases by 10%, the PW increases to the out of the tested range, but the PW decreases to 5.0ns when M_S decreases by 10%.

In comparison with the results in Fig. 10 and Fig. 11, for all impacts of material parameter variation, the quantities of the ΔPW in 40nm diameter is much larger than that in 30nm diameter. The huge gap of ΔPW between the two MTJ diameters is caused by different slope regions of the target RDR. In detail, the corresponding PWs with 30nm MTJ

diameter are located in the steep slope region, on the other hand the PWs with 40nm MTJ diameter are located in the gentle slope. Therefore, the impacts of material parameter variations in 30nm MTJ diameter are limited in relatively narrow range of PW, while the impacts in 40nm MTJ diameter are extended in the wide range of PW. Fig. 12(a) summarizes the impact of all material parameter variations for 30nm and 40nm diameters using the ΔPW in percentage scale. As a result, the read operation in STT-MRAM application can be highly sensitive to the material parameter variations if the required PWs are located in the gentle slope region. Since a positive ΔPW indicates the improvement of the RDR while that the negative ΔPW represents the degradation of the RDR, it is essential to analyze read operation with negative ΔPW as well as the slope region where the target RDR is located. Considering negative ΔPW, the most important variation is M_S, H_K, η, and α in that order, and the relative importance of the material parameter variations should be considered for reliable read operation. Note that decreasing read current can be possible ways to mitigate the degradations of RDR, but the approach can induce other problem such lower sensing margin during read operation.

C. Geometric Parameter Variation in Sensing Operation

The effects of MTJ's geometric parameter variations on RDR are also investigated at 30 nm and 40 nm diameters (Fig. 12(b)). The reduction of t_{OX} induces larger current flowing through the MTJ device, resulting in MTJ flipping with shorter PW. This phenomenon causes RDR degradation. Next, the reduction of t_F or A_F can lessen both I_C and TSF at the same time, therefore the required PW to occur the RD is drastically reduced. Last, the effect of TMR variation on RDR is studied. Since the increase of TMR can enhance spin polarization efficiency factor, η, the RDR rate increases with larger TMR. Compare to 30 nm diameter, there are much larger PW changes with the variations in 40 nm diameter since the required PWs are located in gentle slope region. Fig. 13 shows the RDR degradation with combined MTJ parameter variations at 40 nm diameter. Negative ΔPW means the PW to occur RD with shorter PW, resulting in degradation or increase of RDR rate. Based on the result, the RDR degradation drastically increases even with single degraded variation, especially t_F or A_F, in the worst case and the RDR degradation are slightly increased with more variation sources. As discussed above, especially in 40nm diameter, the RDR rate is very susceptible to the MTJ's material and geometry variations due to its position in the gentle slope region. Not only device level but circuit level research groups should consider the sensitivity of RDR for the reliable sensing operation.

VI. Conclusion

In summary, in order to study the impact of material and geometric parameter variations on the write and read operations as well as the scalability of the MTJ device in STT-MRAM application, we investigated both WER and RDR considering the MTJ material and geometric parameter variations such as M_S, H_K, α, η, t_{OX}, t_F, A_F, and TMR variations in MTJ scaling. In our work, FP numerical solution is mainly used for efficient analysis. Although the impact of all parameter variations on WER is decreased as MTJ scales down from 90 nm to 30 nm, the variation effect can be still critical with small MTJ diameter and the most significant influential variation is η, M_S, H_K, and α in that order. We also show that the material and geometric parameter variations have a tremendous effect on RDR in scaled MTJ diameters (i.e. 30 nm and 40 nm). Especially, the negative variations of H_K, M_S, t_F and A_F can degrade the RDR, resulting in fatal errors for sensing operation. Furthermore, the sensitivity of RDR can be much more sensitive according to the slope region where the target RDR is located in. Therefore, the in-depth study about the material and geometric parameter variations considering relative importance in WER and RDR, and the slope regions with target RDR should be very important to evaluate scalability of MTJ device. Even though STT-MRAM has the diverse potentials for the next-generation universal memory application, such precise investigation into WER and RDR should be completed prior to the commercialization of STT-MRAM applications with compact MTJ devices.

Acknowledgment

This work was supported by Technology Computer-Aided Design (TCAD) group in GLOBALFOUNDRIES, Malta, NY 12020, USA. We thank Dr. Rainer Thoma and Dr. Jeffrey Johnson for their useful discussions and comments during the preparation of this manuscript.

References

[1] D. Apalkov *et al.*, "Spin-transfer Torque Magnetic Random Access Memory (STT-MRAM)," *J Emerg Technol Comput Syst*, vol. 9, no. 2, pp. 13:1–13:35, May 2013.

[2] J. M. Slaughter *et al.*, "Technology for reliable spin-torque MRAM products," *IEEE International Electron Devices Meeting (IEDM)*, pp. 21.5.1-21.5.4., Dec 2016.

[3] C. J. Lin, *et al.*, "45nm low power CMOS logic compatible embedded STT MRAM utilizing a reverse-connection 1T/1MTJ cell," *IEEE International Electron Devices Meeting (IEDM)*, pp. 11.6.1-11.6.4, Dec 2009.

[4] C. Park, *et al.*, "Systematic Optimization of 1 Gbit Perpendicular Magnetic Tunnel Junction Arrays for 28 nm Embedded STT-MRAM and Beyond," *IEEE International Electron Devices Meeting (IEDM)*, pp. 26.2.1-26.2.4., Dec 2015.

[5] Y. Xie, B. Behin-Aein, and A. Ghosh, "Fokker-Planck Study of Parameter Dependence on Write Error Slope in Spin-Torque Switching," *IEEE Transactions on Electron Devices*, vol. 64 , no. 1 , pp. 319-324, Jan 2017.

[6] V. P. K. Miriyala, X. Fong, and G. Liang "FANTASI: A novel devices-to-circuits simulation framework for fast estimation of write error rates in spintronics", *International Conference on Simulation of Semiconductor Processes and Devices (SISPAD)*, Sep 2018.

[7] A. Driskill-Smith, *et al.*, "Latest Advances and Roadmap for In-Plane and Perpendicular STT-RAM," *IEEE International Memory Workshop (IMW),* May 2011.

[8] W. Kim, *et al.*, "Extended scalability of perpendicular STT-MRAM towards sub-20nm MTJ node," *IEEE International Electron Devices Meeting (IEDM)*, pp. 24.1.1-24.1.4., Dec 2011.

[9] T. Andre, *et al.*, "ST-MRAM fundamentals, challenges, and applications," *Proceedings of the IEEE 2013 Custom Integrated Circuits Conference,* Sep 2013.

[10] H. Li et al., "Performance, power, and reliability tradeoffs of STT-RAM cell subject to architecture-level requirement," *IEEE Trans. on Magnetics*, vol. 47, no. 10, pp. 2356-2359, Oct 2011.

[11] N. D. Rizzo, *et al*., "Thermally activated magnetization reversal in submicron magnetic tunnel junctions for magnetoresistive random access memory," Applied Physics Letters, vol. 80, no. 13, pp.2335-2337, Mar 2002.

[12] R. Heindl, A. Chaudhry, and S. E. Russek, ''Estimation of thermal stability factor and intrinsic switching current from switching distributions in spintransfer-torque devices with out-of-plane magnetic anisotropy,'' *AIP Adv.*, vol. 8, no. 1, p. 015011, Jan 2018.

[13] J. Kim, *et al.*, "A technology-agnostic MTJ SPICE model with user-defined dimensions for STT-MRAM scalability studies," *in Proc. Custom Integr. Circuits Conf. (CICC)*, pp. 1–4, Sep 2015.

[14] I. Ahmed, *et al.*, "A comparative study between spin-transfer-torque and spinHall-effect switching mechanisms in PMTJ using SPICE," *IEEE J. Explor. Solid-State Computat. Devices Circuits*, vol. 3, pp. 74–82, Oct 2017.

[15] W. H. Butler *et al.*, "Switching Distributions for Perpendicular Spin-Torque Devices Within the Macrospin Approximation," *IEEE Trans. Magn.*, vol. 48, no. 12, pp. 4684–4700, Dec 2012.

[16] J. J. Nowak *et al.*, "Dependence of Voltage and Size on Write Error Rates in Spin-Transfer Torque Magnetic Random-Access Memory," *IEEE Magnetics Letters*, vol.7, pp.1–4, Mar 2016.

[17] G. Hu *et al.*, "Reliable Five-Nanosecond Writing of Spin-Transfer Torque Magnetic Random-Access Memory," *IEEE Magn. Lett.*, vol. 10, pp.1–4, Jul 2019.

[18] N. Xu *et al.*, "Rare-Failure Oriented STT-MRAM Technology Optimization," in *2018 IEEE Symposium on VLSI Technology*, pp.187–188, Jun 2018.

[19] T. Min, *et al.*, "A Study of Write Margin of Spin Torque Transfer Magnetic Random Access Memory Technology," *IEEE Trans. Magn.*, vol. 46, no. 6, pp.2322–2327, Jun 2010.

[20] M. M. Torunbalci, P. Upadhyaya, S. A. Bhave, and K. Y. Camsari, "Modular Compact Modeling of MTJ Devices," *IEEE Trans. Electron Devices*, pp.4628-4634, Oct 2018.

[21] C. Xu, *et al.*, "Impact of Write Pulse and Process Variation on 22 nm FinFET-Based STT-RAM Design: A Device-Architecture Co-Optimization Approach," *IEEE Trans. on Multi-Scale Computing Systems,* vol. 1, no. 4, pp.195-206, Dec 2015.

[22] Z. Diao, *et al.*, "Spin-transfer torque switching in magnetic tunnel junctions and spin-transfer torque random access memory," *Journal of Physics: Condensed Matter,* vol. 19, no.16, pp.165209.1-165209.13, Apr 2007.

[23] K. Munira, W. H. Butler, and A. W. Ghosh, "A Quasi-Analytical Model for Energy-Delay-Reliability Tradeoff Studies During Write Operations in a Perpendicular STT-RAM Cell," *IEEE Trans. Electron Devices*, vol. 59, no. 8, pp. 2221–2226, Aug. 2012.

[24] M. Aoki, H. Iwasa and Y. Sato., "A Novel Voltage Sensing 1T/2MTJ Cell with Resistance Ratio for Highly Stable and Scalable MRAM," *Digest of Technical Papers. 2005 Symposium on VLSI Circuits,* pp. 170-171, Jun 2005.

[25] W. Kang, et al., "Reconfigurable Codesign of STT-MRAM Under Process Variations in Deeply Scaled Technology," IEEE Transactions on Electron Devices, vol. 62, no. 6, pp.1769-1777, Jun 2015.

[26] Jing Li, Haixin Liu, Sayeef Salahuddin and Kaushik Roy, "Variation-Tolerant Spin-Torque Transfer (STT) MRAM Array for Yield Enhancement," IEEE Custom Intergrated Circuits Conference (CICC), pp.193-196, Sep 2008.

[27] L. Wei, et al., "A 7Mb STT-MRAM in 22FFL FinFET Technology with 4ns Read Sensing Time at 0.9V Using Write-Verify-Write Scheme and Offset-Cancellation Sensing Technique," IEEE International Solid- State Circuits Conference (ISSCC), pp.214-216, Mar 2019.

[28] S. Ikeda, *et al.*, "A perpendicular-anisotropy CoFeB–MgO magnetic tunnel junction," *Nature Materials,* vol. 9, pp.721-724, Jul 2010.

[29] JH. Kim, *et al.*, "Verification on the extreme scalability of STT-MRAM without loss of thermal stability below 15 nm MTJ cell," *Symposium on VLSI Technology (VLSI-Technology): Digest of Technical Papers*, Jun 2014.

[30] Y. Lu, *et al.*, "Fully Functional Perpendicular STT-MRAM Macro Embedded in 40 nm Logic for Energy-efficient IOT Applications," *IEEE International Electron Devices Meeting (IEDM)*, pp.26.1.1-26.1.4., Dec 2015.

[31] H. Liu,, *et al.*, "Time-resolved magnetic relaxation of a nanomagnet on subnanosecond time scales," (2012) [Online]. Available: https://arxiv.org/abs/1205.7034

[32] Y. Zhang, *et al.*, "Electrical Modeling of Stochastic Spin Transfer Torque Writing in Magnetic Tunnel Junctions for Memory and Logic Applications," *IEEE Transactions on Magnetics,* vol. 49, no. 7, pp.4375-4378, Jul 2013.

[33] R. D. Rose, F. Crupi, R. Tomasello, and M. Carpentieri, "A Variation-Aware Timing Modeling Approach for Write Operation in Hybrid CMOS/STT-MTJ Circuits," *IEEE Transactions on Circuits and Systems–I: Regular Papers,* vol. 65, no. 3, pp.1086-1095, Mar 2018.

[34] R. D. Rose, *et al.*, "A Compact Model with Spin-Polarization Asymmetry for Nanoscaled Perpendicular MTJs," *IEEE Transactions on Electron Devices,* vol. 64, no. 10, pp.4346-4353, Oct 2017.

[35] C. Augustine, *et al*., "Design Space Exploration of Typical STT MTJ Stacks in Memory Arrays in the Presence of Variability and Disturbances," IEEE Transactions on Electron Devices, vol. 58, no. 12, pp.4333-4343, Dec 2011.

[36] E. Chen, *et al*., "Advances and Future Prospects of Spin-Transfer Torque Random Access Memory," IEEE Transactions on Magnetics, vol. 46, no. 6, Jun 2010.

[37] W. Kang, *et al.*, "Yield and Reliability Improvement Techniques for Emerging Nonvolatile STT-MRAM," *IEEE Journal on Emerging and Selected Topics in Circuits And Systems,*vol.5, no.1, pp.28-39, Mar 2015.

[38] Y. Zhang, *et al*., "Compact Modeling of Perpendicular-Anisotropy CoFeB/MgO Magnetic Tunnel Junctions," IEEE Transactions on Electron Devices, vol. 59, no. 3, pp.819-826, Mar 2012.

[39] A.V. Khvalkovskiy, *et al*., "Basics principles of the STT-MRAM cell operation in memory arrays," Journal of Physics D: Applied Physics, vol. 46, no. 7, pp.074001-1~074001-20, Jan 2013.

[40] K. Chun, *et al*., "A Scaling Roadmap and Performance Evaluation of In-plane and Perpendicular MTJ Based STT-MRAMs for High-density Cache Memory," IEEE Journal of Solid-State Circuits (JSSC), Feb. 2013.

[41] Y. Zhang, W. Wen, and Y. Chen, "The Prospect of STT-RAM Scaling From Readability Perspective," *IEEE Trans. Magn.*, vol.48, no.11, Nov 2012.

[42] E. K. S. Au, W.-H. Ki, W. H. Mow, S. T. Hung, and C. Y. Wong, "A Novel Current-Mode Sensing Scheme for Magnetic Tunnel Junction MRAM," *IEEE Trans. Magn,* vol. 40, no. 2, pp.483-488, Mar 2004.

[43] J. Song, J. Kim, S. H. Kang, S.-S. Yoon, and S.-O. Jung, "Sensing margin trend with technology scaling in MRAM," *Int. J. Circuit Theory Appl.*, vol. 39, no. 3, pp. 313–325, Mar 2011.

[44] L. Xue, *et al.*, "Process optimization of perpendicular magnetic tunnel junction arrays for last-level cache beyond 7 nm node." *2018 IEEE Symposium on VLSI Technology*. IEEE, 2018.